

---

# CHOOSE YOUR EXPLANATION: A COMPARISON OF SHAP AND GRADCAM IN HUMAN ACTIVITY RECOGNITION

---

 **Felix Tempel**

Faculty of Informatics  
Norwegian University of Science and Technology  
Trondheim, Norway  
felix.e.f.tempel@ntnu.no

 **Daniel Groos**

Faculty of Medicine and Health Sciences  
Norwegian University of Science and Technology  
Trondheim, Norway  
daniel.groos@ntnu.no

 **Espen Alexander F. Ihlen**

Faculty of Medicine and Health Sciences  
Norwegian University of Science and Technology  
Trondheim, Norway  
espen.ihlen@ntnu.no

 **Lars Adde**

Department of Clinical and Molecular Medicine  
Norwegian University of Science and Technology  
Clinic of Rehabilitation  
St. Olavs Hospital, Trondheim University Hospital  
Trondheim, Norway  
lars.adde@ntnu.no

 **Inga Strümke**

Faculty of Informatics  
Norwegian University of Science and Technology  
Trondheim, Norway  
inga.strumke@ntnu.no

December 23, 2024

## ABSTRACT

Explaining machine learning (ML) models using eXplainable AI (XAI) techniques has become essential to make them more transparent and trustworthy. This is especially important in high-stakes domains like healthcare, where understanding model decisions is critical to ensure ethical, sound, and trustworthy outcome predictions. However, users are often confused about which explainability method to choose for their specific use case. We present a comparative analysis of widely used explainability methods, Shapley Additive Explanations (SHAP) and Gradient-weighted Class Activation Mapping (GradCAM), within the domain of human activity recognition (HAR) utilizing graph convolutional networks (GCNs). By evaluating these methods on skeleton-based data from two real-world datasets, including a healthcare-critical cerebral palsy (CP) case, this study provides vital insights into both approaches' strengths, limitations, and differences, offering a roadmap for selecting the most appropriate explanation method based on specific models and applications. We quantitatively and qualitatively compare these methods, focusing on feature importance ranking, interpretability, and model sensitivity through perturbation experiments. While SHAP provides detailed input feature attribution, GradCAM delivers faster, spatially oriented explanations, making both methods complementary depending on the application's requirements. Given the importance of XAI in enhancing trust and transparency in ML models, particularly in sensitive environments like healthcare, our research demonstrates how SHAP and GradCAM could complement each other to provide more interpretable and actionable model explanations.

**Keywords** SHAP, GradCAM, XAI, Explainable AI, Human Activity Recognition, HAR

## 1 Introduction

Significant progress has been made in the development of Graph Convolution Networks (GCNs) for Human Action Recognition (HAR) in recent years. A significant proportion of the research is dedicated to improving the performance of GCN architectures on widely used benchmark datasets, including NTU RGB+D 60/120 [1, 2] and Kinetics [3]. However, less attention has been paid to understanding and explaining the internal workings of the developed architectures. Concurrently, these models' increasing complexity and scale have reduced their interpretability, turning them into "black boxes". Still, understanding the inner workings of such systems is crucial, particularly when they are used in high-risk and sensitive environments such as healthcare, where the outcomes of model decisions can have significant ethical and practical implications [4, 5, 6, 7]. In such contexts, the explainability of models becomes not only a technical concern but also a matter of trust, accountability, and safety [8].

The need for explainability in machine learning (ML) models is pushing the adoption of eXplainable Artificial Intelligence (XAI) techniques to describe the inner workings of GCNs [9]. XAI provides tools for understanding how ML models generate particular predictions to facilitate trust and confidence among end-users and developers. This is done by translating the abstract and high-dimensional concepts underlying these models into a space accessible and comprehensible for humans. XAI is divided into two key categories: interpretability and explainability [10]. Interpretability refers to establishing clear, transparent rules that define how an ML model arrives at its decisions. These insights can then be used for adequate clinical adoption and to reduce the risks emerging from biases in the ML models since physicians can understand the decision process. On the other hand, explainability entails creating a framework that explains the ML model's workings, often by representing its decision-making process in a simplified manner, making it accessible for humans to understand [7].

In domains like healthcare, where decisions can directly impact patient outcomes, the interpretability of ML models used in this field is critical [11, 12, 13]. Clinicians require assurance that ML models produce decisions based on relevant, reliable, and ethically sound data patterns [14]. The lack of interpretability of such systems could lead to dangerous scenarios, including the perpetuation of biases or the incorrect categorization of patient conditions, which might have significant clinical consequences [15, 16]. Therefore, providing explainability by "opening the black box" of GCN-based HAR models is essential for their safe deployment and acceptance in sensitive environments such as healthcare [17].

Despite the increasing relevance of XAI, its application within the HAR domain remains largely underexplored. To the extent that XAI methods have been studied for HAR, these focus primarily on three methods: Shapley Additive Explanations (SHAP) [18, 19], Class Activation Mapping (CAM) [20] and its rectification Gradient-weighted Class Activation Mapping (GradCAM) [21]. Beyond this, there remains a noticeable gap in the literature regarding the systematic comparison of these methods in the HAR field. Specifically, no work has been done to assess which explainability approach is better suited for different types of HAR models and datasets. Further, there is a limited understanding of how different explainability methods vary in their outputs. This gap presents a significant challenge, as the effectiveness and interpretability of XAI methods can vary significantly and depend on the context and model architecture in which they are used. For example, SHAP provides insights into each feature's importance but may fail to capture the spatial and temporal dynamics in the data. GradCAM, on the other side, can highlight important regions for the model but falls short in explaining the contribution of the individual input features. The lack of a comprehensive comparison of these methods with different datasets and HAR model types poses a challenge in identifying the most appropriate methods for model interpretation. Furthermore, clinicians and researchers should be provided with a quantitative comparison of these two XAI methods to assess which is best suited for their individual HAR model, dataset, and use case. Understanding what to expect from each XAI method regarding explanation quality, transparency, and adaptability is essential to making informed decisions. Hence, a systematic comparison of these two XAI methods is needed. This can pave the way for trustworthy HAR models that can be safely and effectively implemented in real-world applications.

### 1.1 Contributions

- Quantitative comparison of SHAP and GradCAM, in the context of HAR with GCN, on skeleton data from two real-world datasets.
- Comparative analysis of the two explanation methods, focusing on feature ranking and evaluating the influence of these features through a perturbation sensitivity analysis on predictive performance.
- A nuanced understanding of the strengths and weaknesses of the two explanation approaches within the HAR domain.

## 2 Related Work

### 2.1 XAI

In the domain of skeleton-based HAR, most XAI techniques rely on saliency-based methods such as CAM [20] or GradCAM [21, 22]. Meanwhile, SHAP, which is widely used in a wide range of ML applications, has received less attention in HAR and was only applied in [18, 19], to the best of our knowledge.

The first work using XAI within HAR is the work from [20]. The authors use CAM to visualize important body key points on the two action classes, *throwing* and *drinking water* from the NTU RGB+D dataset [2]. However, their investigation is restricted to only a qualitative visual representation of the activated body key points for those two action classes. This limits their applicability and quantitative comparability with other techniques. The same authors expand this approach on a refined architecture in [22], where CAM is used again to produce visual explanations. However, these explanations also lack objective evaluation metrics, making comparing their effectiveness with other approaches difficult. Also, a comparison of the activation maps to the earlier work [20] is missing. It can be stated that the CAM approach does not address the contribution of individual input features, an area where SHAP could offer deeper insights. This may be particularly interesting for the architecture used in [22], where the authors use multiple input branches to process features individually before fusing them into a common stream in the model.

In [18], SHAP is applied in a medical context for early cerebral palsy (CP) screening. The model combines video data and secondary features like birth weight, sex, and gestational age to detect fidgety movements, indicating an increased risk for neurological dysfunction if they are absent or sporadic [23]. These features are then classified and combined into a normal and a risk probability for CP. However, the SHAP explanation is limited to the secondary input features, missing the opportunity to explain the primary input features (i.e., the video data). SHAP would also have to be applied to the primary features to properly explain the model, although this represents a greater technical challenge.

Another work using SHAP within the medical HAR domain is [19]. Here, the authors use SHAP to explain the contributions of the primary input features on the model output utilizing two real-world datasets. While this work is the first to apply SHAP on the primary input features, the direct comparison with the often-used GradCAM approach is lacking. A comparison between SHAP and GradCAM could provide a more complete evaluation of the individual strengths and weaknesses. This opens up research on how methods like SHAP and GradCAM might complement or outperform each other in different HAR scenarios and datasets.

## 3 Method

This section outlines the two explainability techniques, SHAP and GradCAM, which are compared in this study. Furthermore, the model architecture used to predict the skeleton data is briefly described, including at which layer we obtain the gradients for GradCAM; see a visualization in Fig. 1. Finally, the perturbation technique used to evaluate the model’s sensitivity is explained, including how specific parts of the architecture are perturbed based on the feature ranking from SHAP and GradCAM.

### 3.1 GradCAM

GradCAM generates an explanation using the gradients from the final convolutional layer of an ML model [24]. To generate explanations, the gradients for class  $c$  are computed with respect to the activations of the feature maps in the chosen convolutional layer. Let  $y^c$  represent the model’s activation for class  $c$  before the chosen target layer, corresponding to the model’s prediction for class  $c$ . The gradients of  $y^c$  with respect to each feature map activation  $A^k$ , where  $A^k$  denotes the  $k$ -th feature map of the final convolutional layer, are then calculated. These gradients indicate how much each spatial location in the feature map contributes to the class prediction. Next, global average pooling is applied to the gradients, yielding the neuron importance weights:

$$\alpha_k^c = \frac{1}{Z} \sum_i \sum_j \frac{\partial y^c}{\partial A_{i,j}^k}, \quad (1)$$

where  $Z$  represents the number of spatial nodes in the feature map  $A^k$ , and  $(i, j)$  are the spatial indices of the feature map. These importance weights  $\alpha_k^c$  reflect the contribution of each feature map to the class prediction.

The final localization map, which highlights the relevant regions in the skeleton, is then computed as follows:

$$L_{\text{GradCAM}}^c = \text{ReLU} \left( \sum_k \alpha_k^c A^k \right), \quad (2)$$

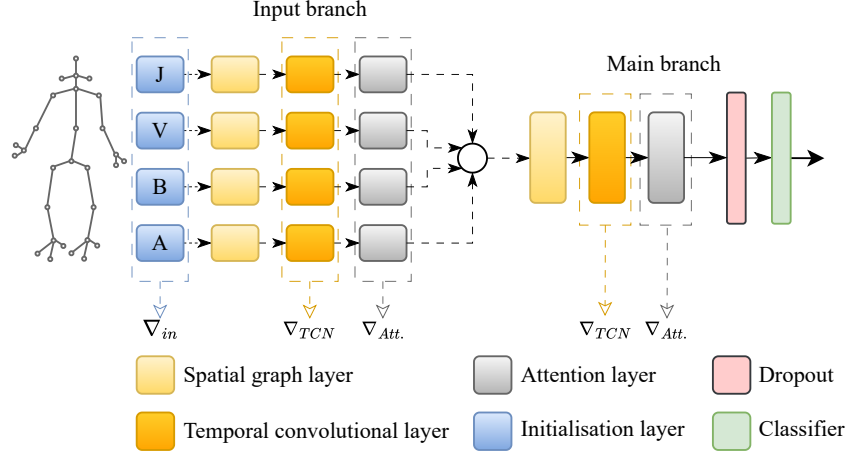


Figure 1: Model architecture with the locations where the gradients are obtained. The model consists of four input branches ( $J, V, B, A$ ) processing different feature divisions obtained from the skeleton video. These features are fused later into a common main branch followed by the classifier. Our reference gradients  $\nabla$  for the experiments are extracted after the attention activation (Att.) and after the temporal convolutional layer (TCN) in the main branch.

where the ReLU activation ensures that only positive contributions (i.e., regions that are positively associated with class  $c$ ) are retained.

We additionally apply the counterfactual explanation, where the gradients are negated [24]. This modification allows us to highlight the areas that decrease the class score, identifying the features that are either less important or negatively contributing to, i.e., contradict, the prediction. This way, we get the negated importance weights via

$$\alpha_k^c = \frac{1}{Z} \sum_i \sum_j - \frac{\partial y^c}{\partial A_{i,j}^k}, \quad (3)$$

and then compute the localization map with (2).

For skeleton-based HAR, GradCAM can be adapted to focus on the relevant spatial-temporal features within the skeletal data. In this context, the skeleton is typically represented as a graph, where nodes correspond to body key points, and edges represent their spatial relations. In GCNs, the final convolutional layer captures the spatial dependencies across the body key points, while the temporal information is encoded across different frames.

In [21], GradCAM is extended to skeleton-based HAR tasks by adapting the method to handle the graph-structured data. Here, the gradients are computed for the graph convolutions, and the localization map indicates which body key points and frames are most influential in the model’s prediction for a specific human activity. This approach can be used to visualize the contributions of different joints and frames, facilitating an understanding of which parts of the body and movement sequences are most relevant for a given activity at a specific time.

### 3.2 SHAP

SHAP is a framework for explaining ML model predictions by attributing an importance score to each feature [25]. It is based on the Shapley value from cooperative game theory [26], which measures a player’s contribution to a team’s overall success. In the context of ML, the Shapley value is adapted to evaluate the impact of each input feature on the model’s prediction. The SHAP value  $\phi_i$  for feature  $i$  is computed as

$$\phi_i = \sum_{S \subseteq F \setminus \{i\}} \frac{|S|!(|F| - |S| - 1)!}{|F|!} [f_{S \cup \{i\}}(x_{S \cup \{i\}}) - f_S(x_S)], \quad (4)$$

where  $S$  represents all subsets of features excluding  $i$ , and  $f_S$  denotes the model’s prediction with the subset  $S$ . Calculating the SHAP value thus requires systematically evaluating the model with and without each feature present. Performing this calculation for all subsets is computationally expensive ( $\mathcal{O}(2^n)$ ), so approximation methods like “Kernel SHAP” and “Deep SHAP” are used to speed up the process [25]. These methods also provide estimation methods for obtaining the model prediction in the absence of input features the model was trained on, as detailed in [25].

The total SHAP value for a model prediction is the sum of individual feature contributions, with the overall prediction approximated as

$$f(x) \approx \sum_{i=1}^N \phi_i(x) + \phi_0. \quad (5)$$

Here,  $\phi_0$  is the expected model output, i.e., the mean prediction across a chosen background dataset. In particular, a feature’s SHAP value quantifies its contribution to driving the model prediction away from the expected or mean prediction.

In our study, features are obtained directly from the skeleton data and categorized into four groups: position ( $J$ ), velocity ( $V$ ), bone ( $B$ ), and acceleration ( $A$ ), further described [27, 28]. The combined SHAP value of a model trained on these features is thus  $\phi = \phi_P + \phi_V + \phi_B + \phi_A$ . The baseline  $\phi_0$  is calculated by averaging over  $n = 100$  randomly sampled data points from the training set  $\mathcal{D}_{train}$ . Although SHAP is computationally expensive, approximations allow for relatively efficient model explanations. Furthermore, the simple decomposition of the SHAP value into input feature importances provides intuitive explanations that yield a certain interpretability of the model. SHAP values can also be aggregated across multiple instances to provide global insights into feature importances across a dataset, helping to identify critical elements influencing model behavior.

### 3.3 Perturbation

Perturbation techniques in XAI are used to analyze model sensitivity by altering input data and observing prediction changes [29]. We use the perturbation technique from [19] to test the two explanation methods and perturb specific parts of the model architecture related to skeleton body key points.

We use GCNs as the backbone of our architectures, which adapt convolutional neural networks to graph data, making them suitable for skeleton-based HAR. In a GCN, nodes aggregate information from neighboring nodes, capturing spatial relationships relevant to human movements. This involves multiplying the node feature matrix by a normalized adjacency matrix  $\mathbf{A}$ , identity matrix  $\mathbf{I}$ , and a learnable edge importance matrix  $\mathbf{E}$ .  $\mathbf{A}$  is then split into  $\mathbf{A}_j$ , such that  $\mathbf{A} + \mathbf{I} = \sum_j \mathbf{A}_j$ . The output is computed as follows [30]:

$$\mathbf{f}_{out} = \sum_j \mathbf{W}_j \mathbf{f}_{in} (\Lambda_j^{-\frac{1}{2}} \mathbf{A}_j \Lambda_j^{-\frac{1}{2}} \odot \mathbf{E}_j) \quad (6)$$

Here,  $\mathbf{f}_{out}$  and  $\mathbf{f}_{in}$  are output and input features.  $\mathbf{W}_j$ ,  $\Lambda_j$ , and  $\mathbf{A}_j$  handle convolution and adjacency matrix normalization, while  $\mathbf{E}$  (learnable diagonal matrix) has the edge importance for the specific body key point.

As in [19], we apply the perturbation by modifying edges  $e_n$  in  $\mathbf{E}$  corresponding to the body key points, using the sorted SHAP and GradCAM values as the importance measure to choose which edge has to be perturbed.

## 4 Experiments

This section thoroughly describes the experiments conducted on the NTU RGB+D and CP datasets. First, we explain the two datasets and outline how they are preprocessed for the model. Then, we give implementation details regarding the GCN model, GradCAM, and SHAP within our framework. Next, we compare how the explainability techniques map importance onto body key points in the skeleton sequences and the overall feature ranking of those. Further, we perform the perturbation experiments to investigate which of the most important body key points, as determined by SHAP and GradCAM, respectively, lead to a more significant decrease in model performance. Also, we correlate GradCAM values from different layers. Finally, we compare the computation time of both explainability methods within our experimental setting.

### 4.1 Datasets

The NTU RGB+D 60 dataset is a 3D human activity dataset widely used for action recognition tasks [2]. It includes 56,880 video samples, categorized into 60 distinct action classes. We use the skeleton mapping of the videos on  $n = 19$  body key points for our experiments [2]. Our experiments focus on the cross-view (X-View) subset as defined in [2]. This subset divides the dataset based on the recorded camera perspectives. Specifically, camera views two and three are used to form the training set,  $\mathcal{D}_{train}$ , while camera view one serves as the validation set,  $\mathcal{D}_{val}$ . For the scope of this study, we explain three action classes performed by a single individual from  $\mathcal{D}_{val}$ .

The second dataset consists of 557 videos featuring infants with medical risk factors for cerebral palsy (CP), recorded between 2001 and 2018 across four countries: the United States ( $n = 248$ ), Norway ( $n = 190$ ), Belgium ( $n = 37$ ), and India ( $n = 82$ ). These videos capture spontaneous movements of infants in a supine position, within the age range of 9 to 18 weeks, and are standardized following the protocols established in [31, 32]. Two medical experts assessed the recordings. Each video frame includes the positions of  $n = 29$  body key points representing the infant’s skeleton, recorded as  $x$  and  $y$  coordinates. The video sequences undergo several preprocessing steps to ensure consistency and improve data quality. These steps include resampling the videos to 30 Hz, applying a median filter to reduce noise, and normalizing the data based on the infant’s trunk length, which serves as a reference point. The normalization involves doubling the trunk length and centering the data at the median mid-pelvis position. After preprocessing, the videos are divided into 5-second windows with a 2.5-second overlap between consecutive windows. The reader is referred to [33] for more details on this dataset.

## 4.2 Implementation

We utilize the best-performing model architecture from [27] for the NTU RGB+D 60 X-View dataset and the architecture from [28] for the CP dataset. In order to compute SHAP values, we apply the “DeepExplainer” from the SHAP library [25]. The “DeepExplainer” algorithm requires a reference dataset representing the underlying data distribution. For this, a random reference set of  $n = 100$  instances is sampled, covering all action classes generated for the NTU RGB+D dataset. Similarly, a reference set consisting of  $n = 100$  randomly selected window samples from both classes is generated for the CP dataset. Since our GPU memory limits the number of background samples that can be processed at once, subsamples of the background ( $n = 20$ ) are used in each experiment, with the resulting SHAP values aggregated afterward. Given the hardware accessibility of typical medical and research institutions, we recommend this as a practical approach. The GradCAM implementation utilizes the PyTorch *registerhook* functionality at the specified layer to acquire the gradients and feature maps [34]. All experiments are conducted on a single NVIDIA V100 GPU with 32 GB of memory, using the PyTorch framework (version 2.3.1) [34] and shap (version 0.46.0) [25]. The global random seed for the experiments is set to 1234.

## 4.3 Qualitative Explanation on Skeleton

In Fig. 2 and 3, the results of the SHAP and the GradCAM values are shown when mapped on the skeleton sequence to visualize their contribution at a specific time frame.

For the NTU RGB+D skeleton, which is taken from class 6 (*Pick up*), it can be observed that the GradCAM activations for the TCN and attention activation layer differ from each other. While the GradCAM values for the TCN layer have a higher portion of activated joints, those from the attention activation layer keep a smaller amount of activated joints. This can be explained by the functionality of the joint attention layer compressing the feature map obtained from the TCN layer to focus on fewer important body key points. Interestingly, the SHAP and GradCAM importance mappings do not agree with each other. For instance, in window 40, SHAP attributes higher importance to the upper body, particularly the head and shoulder regions. Meanwhile, GradCAM emphasizes the left limbs, giving them a higher GradCAM value. This contrast highlights the differing perspectives of these two XAI techniques on which body regions are most crucial for the model’s predictions.

For the CP skeleton analysis, a random infant with CP is selected from the validation set  $\mathcal{D}_{val}$ , and both GradCAM and SHAP values are mapped onto the respective body key points. Notably, the two methods do not always align in their activation of body key points. This discrepancy is evident in window 40, where each method highlights different body regions. However, there is an agreement between SHAP and GradCAM activations in the CP dataset compared to the NTU RGB+D dataset, e.g., in window 10, where both methods give the knees a higher activation. This is potentially due to the smaller window size, which offers more thorough explanations without excessive averaging.

## 4.4 Perturbation

We apply the same perturbation approach as in [19]. Hence, we can directly compare the influence of perturbing important or unimportant body key points on the CP and NTU RGB+D datasets. Furthermore, we apply the negated GradCAM values on the TCN layer from the model for the NTU RGB+D dataset. This way, we can also obtain contributions that negatively influence the prediction of the respective class. For the NTU RGB+D dataset, we chose the same perturbation threshold of 0.35% as in [19] to be able to compare the GradCAM results against the reported SHAP values from this study. In Fig. 4, we show the influence of perturbing up to 10 key body points on the prediction performance for the NTU RGB+D dataset for three classes.

We compare the perturbation results for the NTU RGB+D dataset when taking the TCN and last activation layers’ gradients before the classifier against SHAP. It can be seen that both explanation methods perform better than perturbing

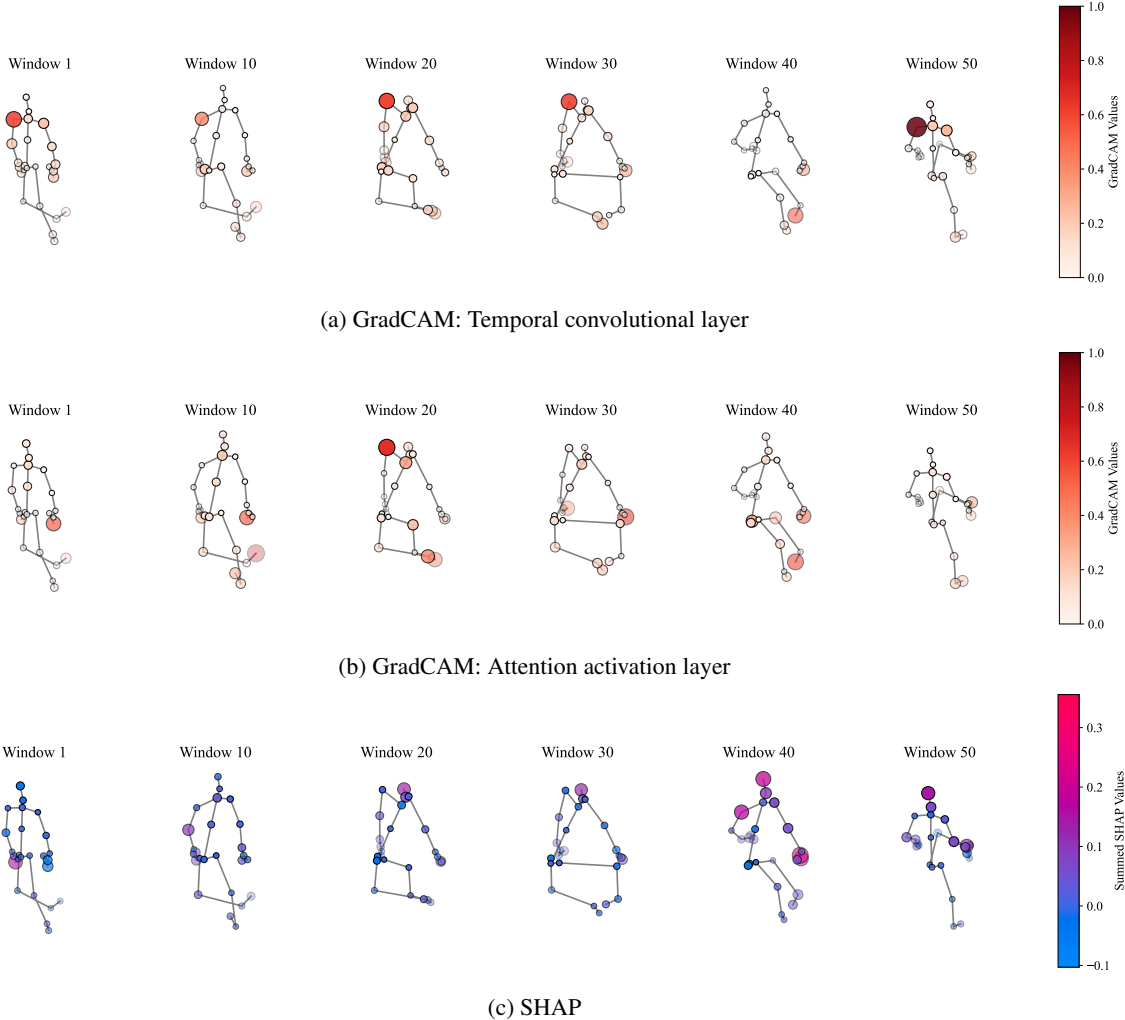


Figure 2: Comparison of the spatial explanations on the body key points with GradCAM for the TCN convolutional layer and attention activation layer, and SHAP for class 6 (*pick up*) of the NTU RGB+D dataset.

edges randomly for important and unimportant features/gradients. Moreover, perturbing important body key points identified using GradCAM outperform those determined by SHAP across all three classes. The performance drop is more significant when using the key points identified by GradCAM, while SHAP shows a smaller degradation when negating gradients or focusing on unimportant features. While SHAP initially performs on par or even better than GradCAM, the performance decline stops at around six perturbed joints for class 6 (*Pick up*) and four for class 16 (*Put on a shoe*). For the experiment with negated gradients for GradCAM and unimportant features for SHAP - SHAP performs better in class 6 but slightly worse in the two other classes.

We evaluate the perturbation experiment using the Area Under the Curve (AUC) metric for the CP dataset, shown in Fig. 5. The results reveal that perturbation of the TCN layer, as assessed through GradCAM values, causes a sharp decline in the AUC curve, particularly after perturbing four body key points. In contrast, perturbation guided by SHAP explanations leads to a steady AUC decline, implicating a correct determination of the important body key points. On the other hand, the perturbation experiments with the GradCAM values taken after the attention layer from the main branch produce erratic results. This unpredictability can be attributed to the CP model’s architecture, where the attention layer primarily focuses on frames and simultaneously activates all joints for an important window. Consequently, the perturbation experiments, which depend on correct spatial information of the important body key points, result in uncorrelated AUC oscillation. In contrast, the joint attention layer for the NTU RGB+D model concentrates on the important body key points rather than time frames, resulting in a smooth performance decrease with the rising number of perturbed edges.

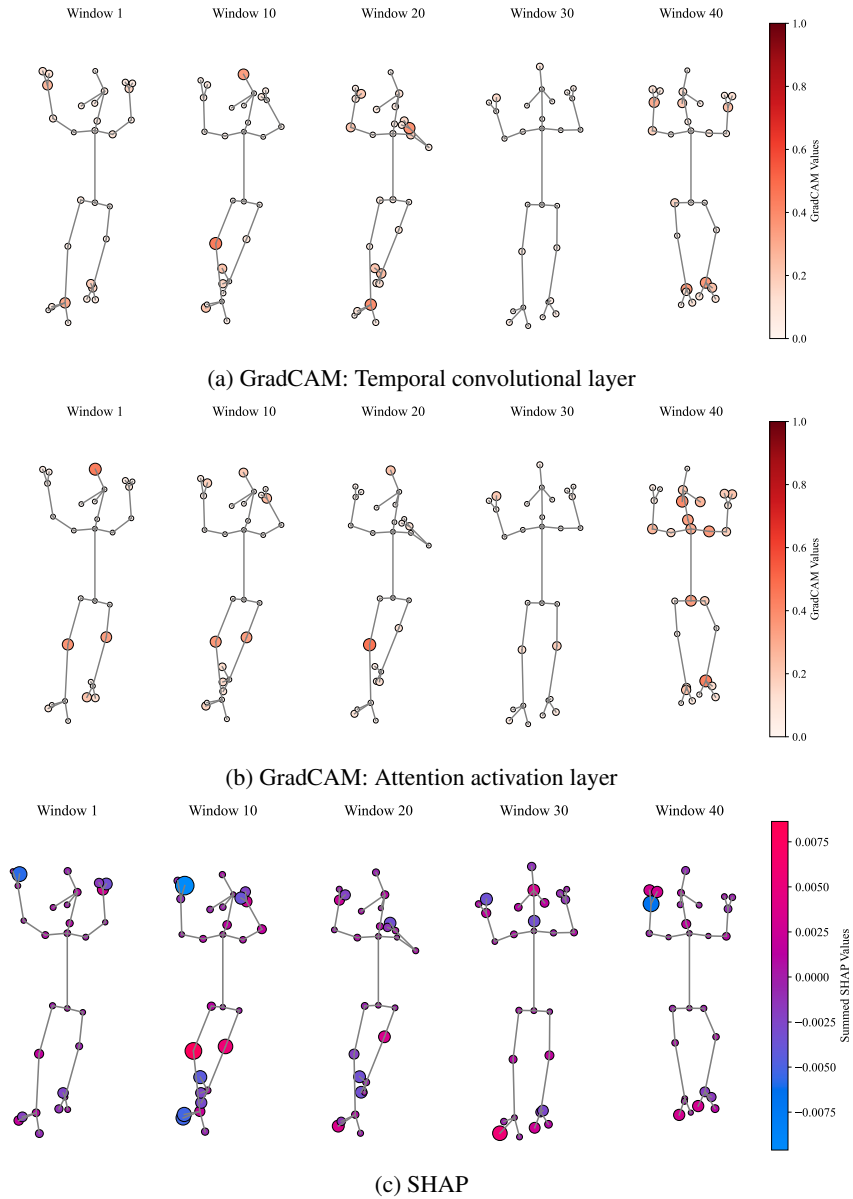


Figure 3: Comparison of the spatial explanations on the body key points with GradCAM for the TCN convolutional and attention activation layers, and SHAP for an infant with CP. The size and color indicate the activation in the respective body key point.



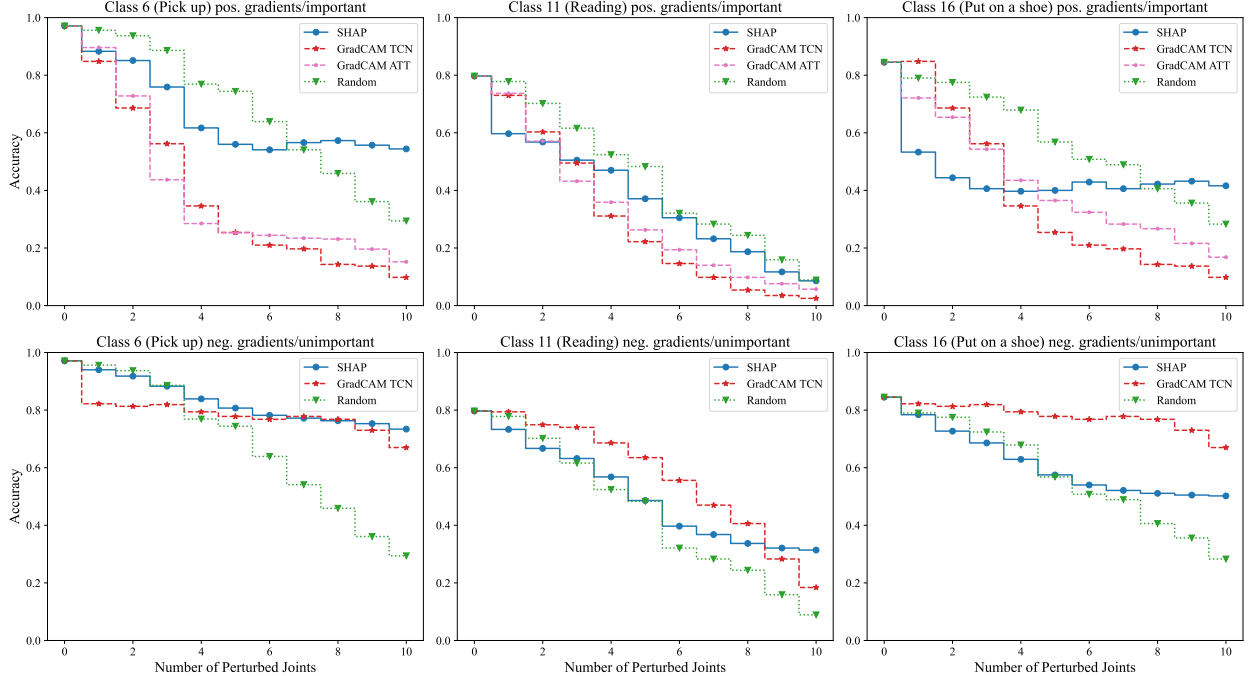


Figure 4: Perturbation experiment results with the three classes from the NTU RGB+D dataset. The first row shows the drop in accuracy if important body key points are perturbed. The second row shows the results when unimportant body key points are perturbed. Both XAI methods perform better than randomly perturbing the body key points, approving their correctness.

#### 4.5 Body key points ranking

We compare both XAI techniques’ body key point ranking for the NTU RGB+D dataset, shown in Fig. 6. It can be seen that SHAP and GradCAM disagree on the ordering of the body key points for the NTU RGB+D dataset. This is likely due to their conceptual difference, where GradCAM gives a more spatial-orientated explanation. Another potential reason for this differing sorting is the averaging technique, where the GradCAM and SHAP values are averaged over the whole sequence. At the same time, SHAP attributes a more general feature contribution to the interactions with other features for a specific body key point. While GradCAM values have a more extensive spread among the different body key points, SHAP, especially for *Class 11*, has a smaller interquartile range from the median.

We apply the same body key point ranking for the GradCAM and SHAP values to one infant with CP and one without CP, shown in Fig. 7. Again, it can be observed that the feature rankings do not agree with SHAP and GradCAM values. Interestingly, the GradCAM values from the frame attention and TCN layers do not agree on their body key point ranking. The same reasons as in Sec. 4.4 can be taken to explain this behavior. As with the NTU RGB+D dataset, the SHAP values have a smaller interquartile range from the median, indicating a higher certainty for the ranking. While SHAP gives the highest importance for the infant with CP to the *right and left knee* with SHAP, the GradCAM values are also the highest in those two body key points for the attention activation layer. For *No CP*, the most critical features, based on the median value, are the *right index finger* and *right knee*, which also align with the TCN GradCAM values.

#### 4.6 GradCAM in Early Layers

To demonstrate the shortcomings of GradCAM in attributing individual input features, we conduct a correlation experiment where GradCAM values are computed for different GCN layers, as shown in Figure 1. We assess the correlation of GradCAM values in 1) initialization layer  $L_{in,i}$ , 2) TCN layer  $L_{TCN,i}$ , and, 3) attention activation layer  $L_{Att.,i}$  of input branches  $i$  to reference values in the attention activation layer of the main branch. We also compute correlation for the sum of input branches ( $L_{in,}$ ,  $L_{TCN,}$ , and  $L_{Att.,}$  respectively) and include in the analysis the TCN layer of the main branch  $m$  ( $L_{TCN,m}$ ).

Similar to [21], layerwise GradCAM values are normalized into the range  $[0, 1]$  before Spearman’s rank correlation coefficient  $\rho$  is computed. Our results in Table 1 show that, for the NTU RGB+D dataset and the CP dataset, GradCAM

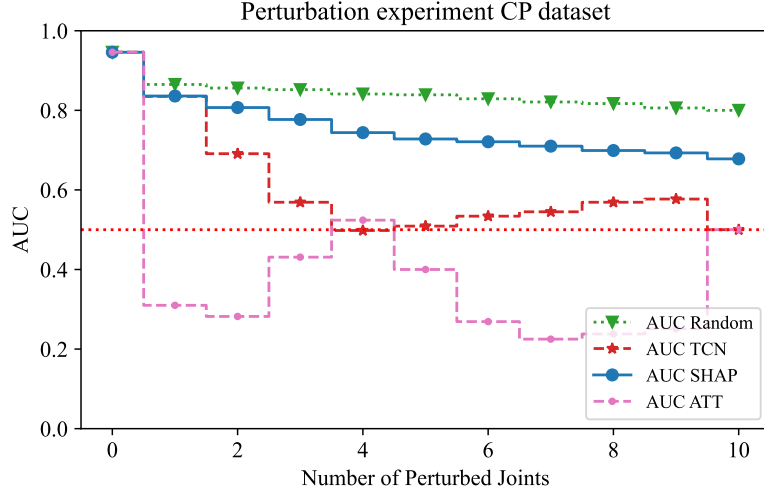


Figure 5: Perturbation results on the CP dataset. Both XAI methods perform better than randomly perturbing body key points, indicating their reliability. The results when the GradCAMs are computed after the frame attention layer perform poorly, indicating that this layer is not well suited for obtaining spatial information.

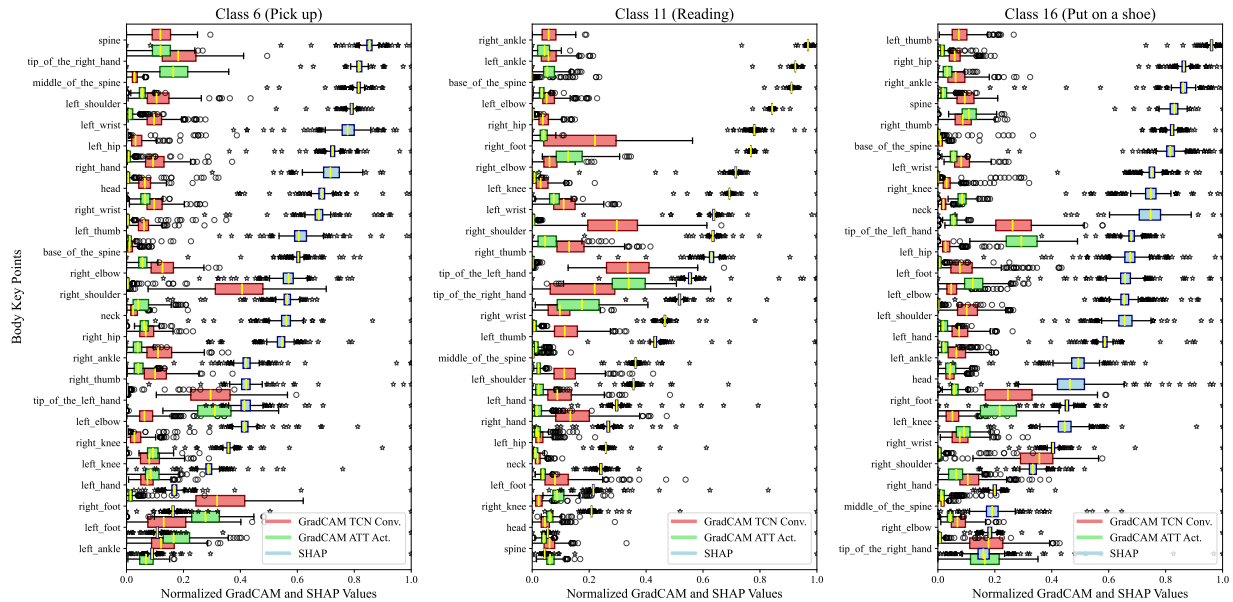


Figure 6: Body key point ranking for the NTU RGB+D dataset on  $n = 316$  instance of three classes taken from  $\mathcal{D}_{val}$ . The plot displays the median and interquartile range and highlights outliers for each body key point and explainability method. The body key points are sorted based on the median of the SHAP values.

values at input branches do not correlate with reference values at the attention activation layer of the main branch. The lack of correlation at input branches of the GCN suggests that SHAP is superior to GradCAM for attributing individual input features (joint, velocity, bone, and acceleration) and specific input channels.

#### 4.7 Runtime

Table 2 lists the computation time for GradCAM and SHAP within our environment. We show the time until the individual algorithm arrives at its final explanation. The GradCAM method is computationally faster than the SHAP method for both datasets due to its lower computational complexity and fewer required calculations. GradCAM only

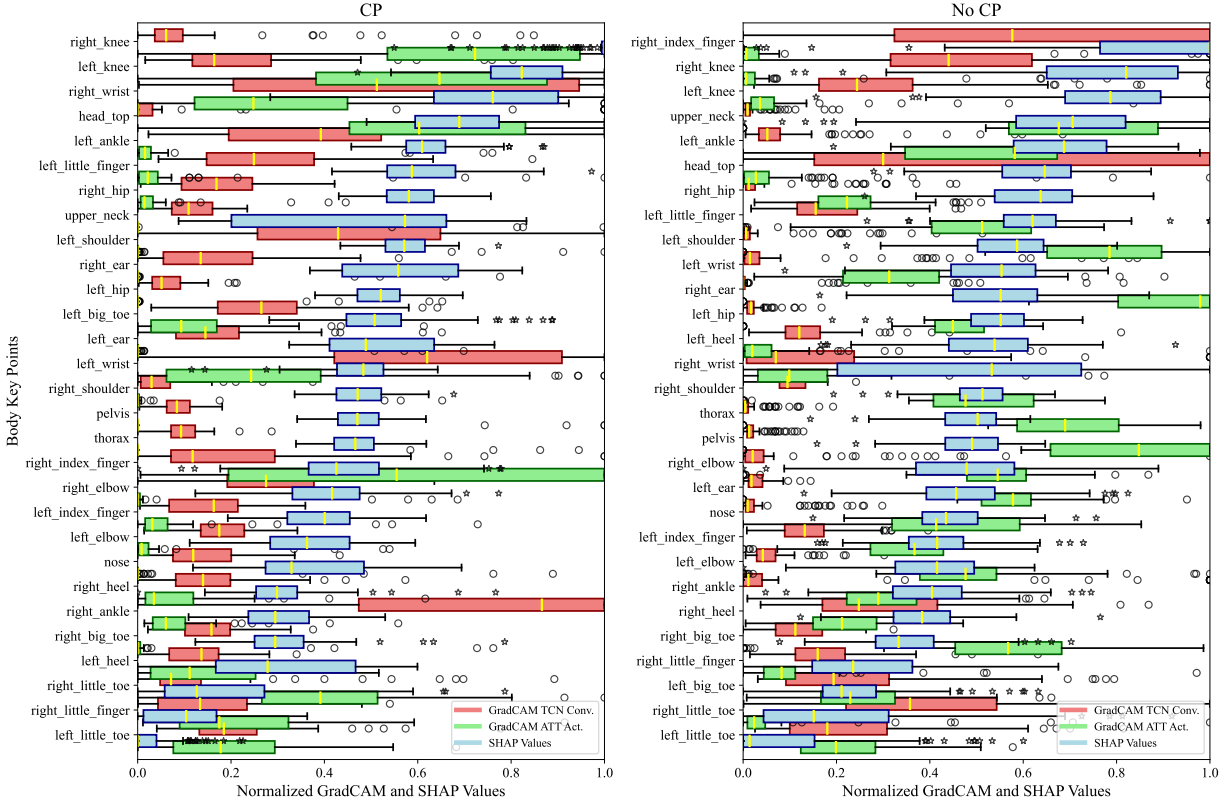


Figure 7: Body key point ranking for one infant with and without CP from  $D_{val}$ . The plot displays the median and interquartile range and highlights outliers for each body key point and explainability method. The body key points are sorted based on the median of the SHAP values.

necessitates one forward and one backward pass of the obtained gradients. On the contrary, SHAP requires multiple propagations of the input data on every feature input. Additionally, the SHAP computation has to be repeated five times in our environment due to memory restrictions to obtain the representative reference dataset of  $n = 100$ . In contrast, SHAP computes the individual feature contribution for all four input features, while GradCAM only provides the gradients of the chosen layer.

## 5 Discussion

Our comparison of SHAP and GradCAM within HAR demonstrates that both methods fundamentally differ in their methodology and the outcome of the final explanation. While they both have unique strengths and weaknesses, their applicability depends heavily on specific needs, requirements, and use cases, which we will elaborate on.

Understanding the model’s decision-making process is crucial in CP diagnosis or treatment planning. SHAP can be used to provide a feature-level explanation, giving clinicians insight into how much each biomechanical feature of each body key point contributes to the model’s final decision. This type of information is highly valuable in clinical settings where practitioners need clear, interpretable reasons behind model outputs. For example, knowing that certain features like acceleration or velocity are more influential in a diagnosis might help to guide the focus on these particular features. GradCAM, on the other hand, provides spatial interpretation, which can be helpful in tasks such as reckoning important body key points in the recording at a specific time frame. It highlights regions of high activation in the model’s chosen target layers, which correspond to body key points in the skeletal structure. This explanation is valuable when clinicians need to visualize which body regions are emphasized, though it lacks the granularity of individual feature importance that SHAP provides.

One significant advantage of SHAP is its ability to depict the importance of opposing features. With SHAP, it is possible to identify which body key points, in combination with the input features ( $J, V, B, A$ ), are essential for the model’s

Table 1: Correlation of GradCAM values obtained from different layers  $L$  for the NTU RGB+D and CP datasets.

Layer	NTU RGB+D	CP
$L_{in,j}$	0.00	0.03
$L_{in,v}$	0.05	0.03
$L_{in,b}$	-0.01	0.02
$L_{in,a}$	0.06	0.03
$L_{in,}$	-0.03	0.04
$L_{TCN,j}$	0.08	0.01
$L_{TCN,v}$	-0.07	-0.06
$L_{TCN,b}$	-0.04	0.01
$L_{TCN,a}$	0.04	-0.01
$L_{TCN,}$	0.00	-0.03
$L_{Att.,j}$	-0.05	-0.14
$L_{Att.,v}$	-0.06	0.11
$L_{Att.,b}$	-0.14	0.10
$L_{Att.,a}$	-0.13	0.16
$L_{Att.,}$	0.00	-0.01
$L_{TCN,m}$	0.24	-0.13

Table 2: Runtime for SHAP and GradCAM explanation on the CP dataset (both classes) and NTU RGB+D X-View (one class) on  $\mathcal{D}_{val}$ . The GradCAM runtime is for one layer, and the SHAP runtime is for one iteration with the reference dataset  $n = 20$ .

Dataset	GradCAM	SHAP
CP	0.35 hours	3.25 hours
NTU RGB+D	0.06 hours	3.22 hours

decision and which are unimportant. While Grad-CAM can show negative importance by reversing gradients, this remains a spatial explanation and lacks the granularity needed for deeper insights.

Another important consideration is the chosen convolutional layer for the GradCAM computation in the model. Our experiments indicate that the last convolutional layer within the network preserved the most information relevant to the final decision. This aligns with prior research recommending focusing on the last convolutional layer for maximal interpretability in Grad-CAM [24]. We also showed that the early-layer activations do not correlate with the activations from the TCN or attention layer, which shows the best results in the perturbation experiment. Furthermore, we obtained the GradCAM values from the frame attention layer for the CP dataset, which focuses on the important time frames rather than the body key points. This may activate body key points, which may no longer provide rich spatial information in some windows. This is due to the attention mechanism, which focuses on the important frames and activates them as a whole instead of the important body key points. When using GradCAM for the activation of the attention layer, the explanation should be interpreted in relation to a specific type of attention (e.g., temporal frame attention versus spatial joint attention), and the architecture of the GCN itself should be modified to emphasize the most useful explanation for the end-user.

Within our study, we applied the perturbation approach from [19], which may be biased towards a spatial-orientated explanation method: GradCAM. Since GradCAM takes the gradients at the specific body key points without needing a reference dataset like SHAP does, it is superior in this specific experimental setting. GradCAM values reflect activation intensities from the chosen layers, which may not be directly comparable to the SHAP feature-based importance values. For example, Grad-CAM highlights regions based on body key point activations, whereas SHAP reflects how much each feature contributes to the model’s output across the entire reference dataset. Additionally, the perturbation method is applied to the whole video frame for the NTU RGB+D data, with the importance scores averaged over the time frame. While this approach provides a general overview of the particular action’s most crucial body key points, it may obscure critical activations of body key points occurring within shorter temporal windows. By averaging the whole video, we risk overlooking nuanced movements or short-duration actions, which are essential for understanding complex human activities. Future work should investigate how a finer temporal averaging technique and localized perturbation strategies can address this limitation. For instance, perturbing the model over smaller, temporally-defined video segments could provide more granular insights. We might capture more precise and contextually relevant perturbations by classifying

shorter video segments and perturbing the network for each segment individually. Such a method could yield more accurate explanations of the model’s behavior, particularly for brief actions involving subtle and short body movements.

SHAP considers feature interactions and how the importance of a body part can change depending on other body parts, while Grad-CAM does not explicitly consider interactions. SHAP provides feature-level attribution, which means it gives importance to the overall contribution of input features and body parts. If a body key point is highly correlated with a particular feature in the model, SHAP might attribute it high importance, regardless of the spatial distribution. SHAP measures how much the body key point contributes to the model’s decision, while Grad-CAM measures how much it contributes to the decision based on its activation. Even if both methods show a body key part as important, the contribution might come from a different context: SHAP values can be influenced by feature interaction and a correlation between the kinematic input features in the model and the underlying reference dataset. In contrast, GradCAM will only consider the direct relationship between the skeleton’s spatial features and the decision. GradCAM hereby examines the regions that activate the most in response to the model’s prediction. It focuses on the body key points where the model’s decision is most influenced, so the resulting heatmap will highlight specific areas that activate the most. However, this might not directly correlate with the feature-level contributions and body key point activations that SHAP captures.

Runtime and computation needs are critical when considering these methods for clinical use. GradCAM’s faster runtime makes it suitable for real-time analysis or applications where speed is essential. SHAP, while slower, provides richer information, making it better suited for offline analysis or in-depth clinical studies where speed and computing resources are less of an issue.

Given these methods’ different strengths and weaknesses, some recommendations can be made for their application in healthcare environments. Grad-CAM might be preferred when a quick, spatial understanding of which body parts the model focuses on is sufficient. This could be useful for real-time diagnostic tools or when working with visual data, such as motion capture or video-based assessments. However, Grad-CAM may miss the ”bigger picture“, ”mainly when interactions between body key points and their features are crucial to the diagnosis and explanation.

While SHAP provides detailed, feature-level explanations, its effectiveness in capturing the true importance of features may be impacted by feature dependencies [35]. SHAP’s default independence assumption may lead to diluted feature importance in scenarios with correlated features, such as the kinematic chain in human motion. GradCAM, with its spatial focus and faster runtime, is more suited to applications where visual feedback and quick assessments are needed. The two methods can complement each other, with SHAP giving the ”why“ behind model decisions and Grad-CAM giving the ”where.“ In conclusion, the explainability of an ML model should always be tailored to different stakeholders, providing each with an appropriate level of detail based on their specific needs [11].

## 6 Conclusion

This paper systematically compared SHAP and GradCAM within the context of GCNs and HAR using skeleton data from two real-world datasets. Our findings highlight that these two explainability methods differ in their approach and output, each offering different benefits depending on the specific requirements of the individual use case.

SHAP provides a detailed, feature-level explanation, making it practical in scenarios where it is crucial to understand each individual body’s key points’ contribution in combination with the input features. It offers a more profound, finer view of how specific features impact the model’s decisions, which is essential for trust and accountability in sensitive domains. This may be required in healthcare applications such as CP prediction, where decisions must be transparent and explainable to clinicians. However, its computational intensity and longer runtime make it less suitable for real-time applications.

In contrast, GradCAM provides quicker, spatially oriented explanations, showing which regions of the body are most influential in the model’s decision at a specific time frame. Its speed and simplicity make it a better choice for real-time assessments or scenarios where quick and more straightforward visual feedback is necessary. However, its lack of granularity and inability to capture complex feature interactions from earlier layers limits its effectiveness in circumstances demanding deeper insights.

Nevertheless, our study demonstrates that SHAP and GradCAM should be viewed as complementary tools rather than competing methods. SHAP provides the ”why“ behind decisions, while GradCAM offers the ”where.“ Depending on the specific demands of the task, whether it is the need for quick, spatial understanding or a thorough, feature-level interpretation, these methods can be used in parallel to provide a more complete and interpretable explanation of the model behavior on the dataset. For future work, hybrid approaches that combine the strengths of both SHAP and GradCAM should be explored. We can enhance these systems’ safety, transparency, and trustworthiness by tailoring explainability techniques to specific HAR models and datasets, particularly in high-risk domains like healthcare.

## Contributions

**Felix Tempel:** Conceptualization; Methodology; Formal analysis; Software; Writing - original draft preparation. **Daniel Groos:** Formal analysis; Methodology; Writing Sec. 4.6 - review and editing. **Espen Alexander F. Ihlen:** Data curation; Supervision; Writing - review and editing. **Lars Adde:** Conceptualization; Data curation; Writing - review and editing. **Inga Strümke:** Project administration; Supervision; Writing - review and editing.

## Data Availability

The NTU RGB + D 60 dataset supporting the findings of this study is available at <https://rose1.ntu.edu.sg/dataset/actionRecognition/> [2]. Due to ethical considerations, the CP dataset is not publicly available.

## Code availability

The code and the experimental results are publicly available at <https://github.com/DeepInMotion/ShapGCN>

## Acknowledgements

This work was partly supported by the PERSEUS Project, a European Union’s Horizon 2020 Research and Innovation Program under the Marie Skłodowska-Curie under Grant 101034240, and partly by the Research Council of Norway under Grant 327146.

## References

- [1] Jun Liu et al. “NTU RGB+D 120: A Large-Scale Benchmark for 3D Human Activity Understanding”. In: *IEEE Transactions on Pattern Analysis and Machine Intelligence* 42.10 (2020), pp. 2684–2701. DOI: 10.1109/TPAMI.2019.2916873.
- [2] Amir Shahroudy et al. *NTU RGB+D: A Large Scale Dataset for 3D Human Activity Analysis*. Apr. 2016. arXiv: 1604.02808.
- [3] Will Kay et al. *The Kinetics Human Action Video Dataset*. 2017. arXiv: 1705.06950 [cs.CV].
- [4] Subrato Bharati, M. Rubaiyat Hossain Mondal, and Prajoy Podder. “A Review on Explainable Artificial Intelligence for Healthcare: Why, How, and When?”. In: *IEEE Transactions on Artificial Intelligence* 5.4 (Apr. 2024), pp. 1429–1442. DOI: 10.1109/TAI.2023.3266418.
- [5] Ahmad Chaddad et al. “Survey of Explainable AI Techniques in Healthcare”. In: *Sensors* 23.2 (Jan. 2023), p. 634. DOI: 10.3390/s23020634.
- [6] Hui Wen Loh et al. “Application of Explainable Artificial Intelligence for Healthcare: A Systematic Review of the Last Decade (2011–2022)”. In: *Computer Methods and Programs in Biomedicine* 226 (Nov. 2022), p. 107161. DOI: 10.1016/j.cmpb.2022.107161.
- [7] Zahra Sadeghi et al. “A Review of Explainable Artificial Intelligence in Healthcare”. In: *Computers and Electrical Engineering* 118 (Aug. 2024), p. 109370. DOI: 10.1016/j.compeleceng.2024.109370.
- [8] Erico Tjoa and Cuntai Guan. “A Survey on Explainable Artificial Intelligence (XAI): Toward Medical XAI”. In: *IEEE Transactions on Neural Networks and Learning Systems* 32.11 (Nov. 2021), pp. 4793–4813. DOI: 10.1109/TNNLS.2020.3027314.
- [9] Grégoire Montavon, Wojciech Samek, and Klaus-Robert Müller. “Methods for Interpreting and Understanding Deep Neural Networks”. In: *Digital Signal Processing* 73 (Feb. 2018), pp. 1–15. DOI: 10.1016/j.dsp.2017.10.011.
- [10] Varad Vishwarupe et al. “Explainable AI and Interpretable Machine Learning: A Case Study in Perspective”. In: *Procedia Computer Science* 204 (2022), pp. 869–876. DOI: 10.1016/j.procs.2022.08.105.
- [11] Petra Korica, Neamat El Gayar, and Wei Pang. “Explainable Artificial Intelligence in Healthcare: Opportunities, Gaps and Challenges and a Novel Way to Look at the Problem Space”. In: *Intelligent Data Engineering and Automated Learning – IDEAL 2021*. Ed. by Hujun Yin et al. Vol. 13113. Cham: Springer International Publishing, 2021, pp. 333–342. DOI: 10.1007/978-3-030-91608-4\_33.
- [12] Johannes Allgaier et al. “How Does the Model Make Predictions? A Systematic Literature Review on the Explainability Power of Machine Learning in Healthcare”. In: *Artificial Intelligence in Medicine* 143 (Sept. 2023), p. 102616. DOI: 10.1016/j.artmed.2023.102616.

- [13] Sajid Nazir, Diane M. Dickson, and Muhammad Usman Akram. “Survey of Explainable Artificial Intelligence Techniques for Biomedical Imaging with Deep Neural Networks”. In: *Computers in Biology and Medicine* 156 (Apr. 2023), p. 106668. DOI: 10.1016/j.combiomed.2023.106668.
- [14] Saranya A. and Subhashini R. “A Systematic Review of Explainable Artificial Intelligence Models and Applications: Recent Developments and Future Trends”. In: *Decision Analytics Journal* 7 (June 2023), p. 100230. DOI: 10.1016/j.dajour.2023.100230.
- [15] Julie Gerlings, Millie Søndergaard Jensen, and Arisa Shollo. “Explainable AI, but Explainable to Whom? An Exploratory Case Study of xAI in Healthcare”. In: *Handbook of Artificial Intelligence in Healthcare: Vol 2: Practicalities and Prospects* (2022), pp. 169–198. DOI: 10.1007/978-3-030-83620-7\_7.
- [16] Christopher J. Kelly et al. “Key Challenges for Delivering Clinical Impact with Artificial Intelligence”. In: *BMC Medicine* 17.1 (Dec. 2019), p. 195. DOI: 10.1186/s12916-019-1426-2.
- [17] Alfredo Vellido. “The Importance of Interpretability and Visualization in Machine Learning for Applications in Medicine and Health Care”. In: *Neural Computing and Applications* 32.24 (Dec. 2020), pp. 18069–18083. DOI: 10.1007/s00521-019-04051-w.
- [18] Qiang Gao et al. “Automating General Movements Assessment with Quantitative Deep Learning to Facilitate Early Screening of Cerebral Palsy”. In: *Nature Communications* 14.1 (Dec. 2023), p. 8294. DOI: 10.1038/s41467-023-44141-x.
- [19] Felix Tempel et al. *Explaining Human Activity Recognition with SHAP: Validating Insights with Perturbation and Quantitative Measures*. 2024. DOI: 10.48550/ARXIV.2411.03714.
- [20] Yi-Fan Song et al. “Stronger, Faster and More Explainable: A Graph Convolutional Baseline for Skeleton-based Action Recognition”. In: *Proceedings of the 28th ACM International Conference on Multimedia*. Seattle WA USA: ACM, Oct. 2020, pp. 1625–1633. DOI: 10.1145/3394171.3413802.
- [21] Pratyusha Das and Antonio Ortega. “Gradient-Weighted Class Activation Mapping for Spatio Temporal Graph Convolutional Network”. In: *ICASSP 2022 - 2022 IEEE International Conference on Acoustics, Speech and Signal Processing (ICASSP)*. Singapore, Singapore: IEEE, May 2022, pp. 4043–4047. DOI: 10.1109/ICASSP43922.2022.9746621.
- [22] Yisheng Song et al. “Constructing Stronger and Faster Baselines for Skeleton-Based Action Recognition”. In: *IEEE transactions on pattern analysis and machine intelligence* PP (2022). DOI: 10.1109/TPAMI.2022.3157033.
- [23] Christa Einspieler, Robert Peharz, and Peter B. Marschik. “Fidgety Movements – Tiny in Appearance, but Huge in Impact”. In: *Jornal de Pediatria* 92.3 (May 2016), S64–S70. DOI: 10.1016/j.jped.2015.12.003.
- [24] Ramprasaath R. Selvaraju et al. “Grad-CAM: Visual Explanations from Deep Networks via Gradient-based Localization”. In: *International Journal of Computer Vision* 128.2 (Feb. 2020), pp. 336–359. DOI: 10.1007/s11263-019-01228-7.
- [25] Scott Lundberg and Su-In Lee. *A Unified Approach to Interpreting Model Predictions*. Nov. 2017. arXiv: 1705.07874 [cs, stat].
- [26] L. Shapley. “7. A Value for n-Person Games. Contributions to the Theory of Games II (1953) 307-317.” In: *Classics in Game Theory*. Ed. by Harold William Kuhn. Princeton University Press, Dec. 1997, pp. 69–79. DOI: 10.1515/9781400829156-012.
- [27] Felix Tempel, Espen Alexander F. Ihlen, and Inga Strümke. “AutoGCN-toward Generic Human Activity Recognition with Neural Architecture Search”. In: *IEEE access : practical innovations, open solutions* 12 (2024), pp. 39505–39516. DOI: 10.1109/ACCESS.2024.3377103.
- [28] Felix Tempel, Espen Alexander F. Ihlen, and Inga Strümke. *Lightweight Neural Architecture Search for Cerebral Palsy Detection*. Sept. 2024. arXiv: 2409.20060 [cs].
- [29] Haoyi Xiong et al. *Towards Explainable Artificial Intelligence (XAI): A Data Mining Perspective*. Jan. 2024. arXiv: 2401.04374 [cs].
- [30] Sijie Yan, Yuanjun Xiong, and Dahua Lin. “Spatial Temporal Graph Convolutional Networks for Skeleton-Based Action Recognition”. In: *Thirty-second AAAI conference on artificial intelligence* (Jan. 2018). arXiv: 1801.07455.
- [31] Heinz FR Prechtl et al. “An Early Marker for Neurological Deficits after Perinatal Brain Lesions”. In: *The Lancet* 349.9062 (May 1997), pp. 1361–1363. DOI: 10.1016/S0140-6736(96)10182-3.
- [32] Christa Einspieler, Heinz F. R. Prechtl, and Arend F. Bos. *Prechtl’s Method on the Qualitative Assessment of General Movements in Preterm, Term and Young Infants*. London: Mac Keith Press, 2004.
- [33] Daniel Groos et al. “Development and Validation of a Deep Learning Method to Predict Cerebral Palsy From Spontaneous Movements in Infants at High Risk”. In: *JAMA Network Open* 5.7 (July 2022), e2221325. DOI: 10.1001/jamanetworkopen.2022.21325.

- [34] Adam Paszke et al. *PyTorch: An Imperative Style, High-Performance Deep Learning Library*. Dec. 2019. arXiv: 1912.01703 [cs, stat].
- [35] Kjersti Aas, Martin Jullum, and Anders Løland. “Explaining Individual Predictions When Features Are Dependent: More Accurate Approximations to Shapley Values”. In: *Artificial Intelligence* 298 (Sept. 2021), p. 103502. DOI: 10.1016/j.artint.2021.103502.